INL/CON-16-40387
PREPRINT

SOLVING CONJUGATE HEAT TRANSFER PROBLEM IN TWO-PHASE FLOW USING NEWTON-KRYLOV METHOD

The 17th International Topical Meeting on Nuclear Reactor Thermal Hydraulics (NURETH-17)

Ling Zou, Haihua Zhao, Hongbin Zhang, Guojun Hu

January 2017

The INL is a
U.S. Department of Energy
National Laboratory
operated by
Battelle Energy Alliance

SOLVING CONJUGATE HEAT TRANSFER PROBLEM IN TWO-PHASE FLOW USING NEWTON-KRYLOV METHOD

Ling Zou, Haihua Zhao, Hongbin Zhang
Idaho National Laboratory
P.O. Box 1625, Idaho Falls, ID 83415-3870 USA
ling.zou@inl.gov; haihua.zhao@inl.gov; hongbin.zhang@inl.gov

Guojun Hu
Department of Nuclear, Plasma, and Radiological Engineering
University of Illinois at Urbana-Champaign, Urbana, IL 61801 USA
ghu3@illinois.edu

ABSTRACT

In this paper, we demonstrated a successful application to use Newton-Krylov method in solving conjugate heat transfer problem in two-phase flow in a fully coupled and fully implicit manner. Such a problem represents the most fundamental physics, i.e., heat transfer between fuel rods and reactor coolant during postulated accidental scenarios, in nuclear reactor safety analysis. The two-phase flow is modeled with the one-dimensional two-fluid two-phase flow model that is widely used in system analysis codes. The heat conduction is modeled with a two-dimensional heat conduction model. For spatial discretization, staggered grid upwind finite volume method is used for flow equations. First-order and second-order schemes (an extension to the first-order scheme) are both available. The standard second-order finite differencing method is used for the two-dimensional heat conduction model. For time integration, both the fully implicit first-order backward Euler (BDF1) and second-order BDF2 schemes are provided. Several treatments were also introduced to enhance the robustness of the Newton-Krylov method in solving such a non-linear problem that is discontinuous in nature because of the discrete closure correlations. These treatments include the re-consideration of a transition region between the slug and annular mist flow regimes, and a simplification made in the interfacial drag term. Numerical results have been extensively validated with experimental data in both pipe and rod bundle geometries, and with a wide range of thermal-hydraulics conditions, including pressure, inlet mass flow rate and subcooling, wall heat flux, and outlet void fraction. Further code-to-code benchmark with the RELAP5-3D code provides further evidence on the correct implementation of wall heat transfer models.

KEYWORDS
Two-phase flow, heat conduction, Jacobian-free Newton Krylov method

1. INTRODUCTION

In nuclear reactor safety analysis, conjugate heat transfer between fuel rods and reactor coolant is essential to the accurate prediction of the peak cladding temperature during postulated accidents, such as the loss of coolant accident (LOCA). In existing codes, such as RELAP5 [1], these two parts of nonlinearly coupled physics, i.e., two-phase flow and heat conduction, are solved in separate linear systems, which introduces additional numerical errors [2]. For numerical simulations on fast or long transient reactor accidents, it is desirable to employ fully coupled and fully implicit methods in order to reduce numerical errors. In the pioneering work of Mousseau [2], a Jacobian-free Newton Krylov (JFNK)

method was used to solve a conjugate two-phase flow and heat conduction problem. Numerical error analysis was given in details for the fully implicit method, which demonstrated several orders of magnitude smaller numerical errors compared to the semi-implicit method. Following Mousseau's pioneering studies, a series of systematic studies were carried out previously to investigate the applicability of JFNK method in solving two-phase flow problems when the phase appearance/disappearance phenomenon [3-4] and realistic closure correlations are considered [5]. Although much successful experience has been obtained in these studies, it is a critical task to extend such studies to include the heat conduction model and the wall heat transfer model that are essential to reactor safety analysis. It is critical to investigate the applicability and solver performance of the JFNK method in such an application, given the high complexity and discontinuous nature of wall boiling heat transfer models.

2. FIELD EQUATIONS

Figure 1 (a) shows a typical conjugate heat transfer model between a fuel rod and its surrounding coolant flow that resembles the flow and heat transfer conditions in nuclear reactor cores. In order to accurately predict the thermal-hydraulics conditions, such as axial void fraction distribution and peak cladding temperature, both the two-phase flow in the flow channel and heat conduction in the fuel rod have to be correctly modeled. In reactor safety analysis codes, the two-phase flow in the channel is normally modeled as one-dimensional flow due to the very large length-to-diameter aspect ratio, while the heat conduction in the fuel rod is modeled using either one-dimensional or multi-dimensional heat conduction equation, depending on the specific scenarios. In the following sections, the commonly used two-fluid two-phase flow model and two-dimensional heat conduction equation, as well as closure correlations to close the equation system, will be discussed.

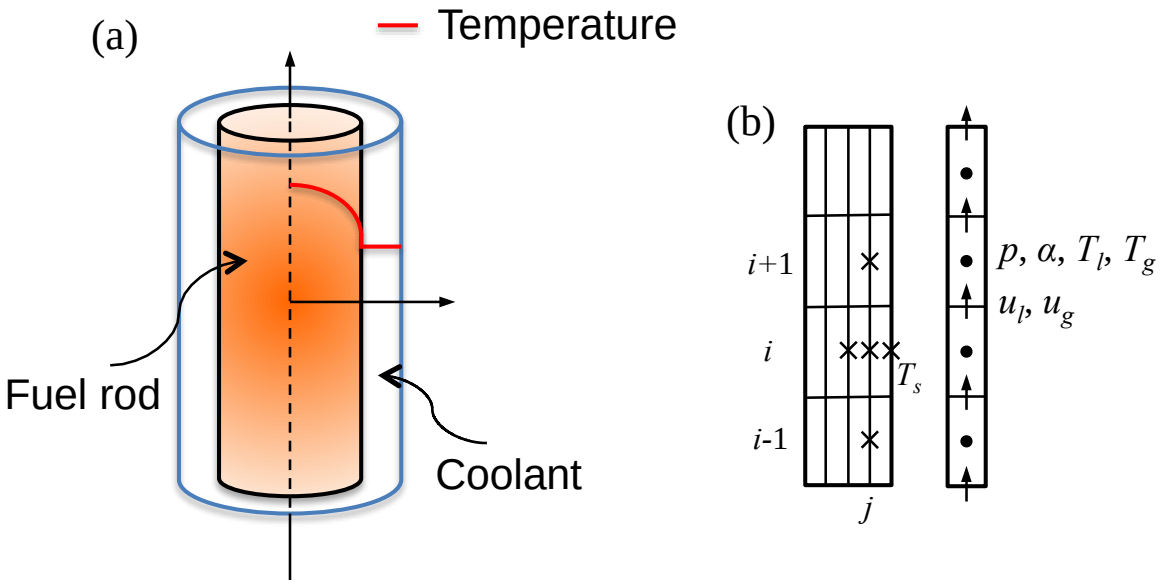

Figure 1, (a) Schematic drawing of the conjugate heat transfer between a fuel rod and its surrounding coolant; (b) Mesh and variable arrangements for both the one-dimensional two-phase model and two-dimensional heat conduction model.

2.1 Field Equations

For the two-phase flow model, the single-pressure two-fluid six-equation model has been used in this paper. Such a two-fluid model is widely used in many existing nuclear reactor system analysis codes,

including RELAP5 [1], TRAC [6], TRACE [7], and CATHARE [8]. It is well known that the basic equation set of the two-fluid model is mathematically ill-posed (lack of hyperbolicity), and different treatments were proposed to render the equations system to be hyperbolic. Such treatments include, for example, the virtual mass term used in the RELAP5 code [1], and the interfacial pressure term used in the CATHARE code [8]. Such treatment terms are, however, excluded in this paper for the purpose of simplicity. The basic set of the six-equation system includes a set of mass, momentum, and energy equations for each phase. They are summarized as,

$$\frac{\partial(\alpha_l\rho_l)}{\partial t}+\frac{\partial(\alpha_l\rho_l u_l)}{\partial x}=-\Gamma_g \tag{1}$$

$$\frac{\partial(\alpha_g\rho_g)}{\partial t}+\frac{\partial(\alpha_g\rho_g u_g)}{\partial x}=\Gamma_g \tag{2}$$

$$\alpha_l\rho_l\frac{\partial u_l}{\partial t}+\alpha_l\rho_l u_l\frac{\partial u_l}{\partial x}+\alpha_l\frac{\partial p}{\partial x}-\alpha_l\rho_l g_x-F_{int}+F_{wall,l}+\Gamma_g(u_{int}-u_l)=0 \tag{3}$$

$$\alpha_g\rho_g\frac{\partial u_g}{\partial t}+\alpha_g\rho_g u_g\frac{\partial u_g}{\partial x}+\alpha_g\frac{\partial p}{\partial x}-\alpha_g\rho_g g_x+F_{int}+F_{wall,g}-\Gamma_g\left(u_{int}-u_g\right)=0 \tag{4}$$

$$\frac{\partial(\alpha_l\rho_l e_l)}{\partial t}+\frac{\partial(\alpha_l\rho_l u_l e_l)}{\partial x}+p\frac{\partial\alpha_l}{\partial t}+p\frac{\partial(\alpha_l u_l)}{\partial x}-Q_{wl}-Q_{il}+\Gamma_{ig}h_l^*+\Gamma_w h_l'=0 \tag{5}$$

$$\frac{\partial\left(\alpha_g\rho_g e_g\right)}{\partial t}+\frac{\partial\left(\alpha_g\rho_g u_g e_g\right)}{\partial x}+p\frac{\partial\alpha_g}{\partial t}+p\frac{\partial\left(\alpha_g u_g\right)}{\partial x}-Q_{wg}-Q_{ig}-\Gamma_{ig}h_g^*-\Gamma_w h_g'=0 \tag{6}$$

in which, subscripts l and g denote the liquid phase and the gas phase, respectively; and subscript '*int*' denotes the two-phase interface. Γ_g is net vapor generation rate due to wall boiling/condensation (Γ_w), and bulk evaporation/condensation (Γ_{ig}). $F_{wall,l}$ and $F_{wall,g}$ represent wall friction terms for the liquid phase and the vapor phase, respectively. Q_{wl} and Q_{wg} are wall-to-liquid and wall-to-gas phase heat transfer terms, respectively. Q_{il} and Q_{ig} are the interface-to-liquid and interface-to-gas phase heat transfer terms, respectively. h_l' and h_g' are phasic enthalpy carried by wall vapor generation term. h_l^* and h_g^* are phasic enthalpy carried by interfacial mass transfer term. The variables to be solved from this set of equations, in the vector form, are $\boldsymbol{U}=[p,\ \alpha_g,\ u_l,\ u_g,\ T_l,\ T_g]^{\mathrm{T}}$, which are pressure, void fraction (volume fraction of the gas phase), liquid phase velocity, gas phase velocity, liquid phase temperature, and gas phase temperature, respectively. The thermodynamic properties of each phase, such as density and specific internal energy, are determined as functions of pressure and phasic temperature, e.g., $e = e(p, T)$. In addition, it is noted that, $\alpha_l + \alpha_g = 1$.

The heat conduction in solid heat structures is modeled with the two-dimensional heat conduction equations in Cartesian coordinates,

$$\rho_s c_{p,s}\frac{\partial T_s}{\partial t}-\frac{\partial}{\partial x}\left(k_s\frac{\partial T_s}{\partial x}\right)-\frac{\partial}{\partial y}\left(k_s\frac{\partial T_s}{\partial y}\right)-q_s'''=0 \tag{7}$$

in which, subscript s denotes solid heat structure; ρ, c_p, T, and k are density, heat capacity, temperature, and thermal conductivity of the solid heat structure, respectively. q_s''' is the volumetric heat source in heat structure. The coupling between the fluid energy equation and the heat conduction equation is through the wall heat transfer terms in the fluid energy equations and the boundary conditions for the heat conduction equations, i.e.,

$$-k_s\frac{\partial T_s}{\partial y}=q_w'' \tag{8}$$

where q''_w is wall heat flux to the two-phase flow due to convection, boiling, and etc. In conjugate heat transfer, this quantity is determined from wall heat transfer coefficient, wall and fluid temperatures. Wall heat transfer coefficient is modeled as closure correlations, which will be discussed in the next section.

2.2 Closure Correlations

Additional closure correlations are needed to close the equations system, including correlations to determine local flow regimes, heat transfer and friction between the heat structure (wall) and fluids, interfacial friction and heat and mass transfer. Since most of these closure correlations have been well discussed in our previous paper [5], they will only be briefly discussed here. We will focus on the additional closure correlations, i.e., wall heat transfer closure correlations, and the interfacial friction model that has also been simplified in this paper.

In this paper, it is the pre-CHF (critical heat flux) two-phase flow regimes in vertical flow channels (tube or rod bundle) that are of interest, and therefore implemented. Similar to RELAP5-3D [9], these vertical flow regimes include bubbly flow, slug flow, annular mist flow, and mist flow pre-CHF in the two-phase flow region. An additional single-phase liquid flow regime is also included. The transition between the single-phase flow to two-phase flow has been discussed in two previous papers [3,4]. In each finite volume, flow regime is determined from local geometry and thermal-hydraulics conditions, such as void fraction, phasic densities, phasic velocities, pipe diameter, and etc. The closure correlations for determining flow regimes are well documented in the RELAP5-3D code manual [9] and our previous paper [5], and therefore are omitted here.

Wall friction is calculated for both the single-phase and two-phase flow conditions. For single-phase conditions, wall friction is modeled in laminar flow, turbulent flow, and a transition flow regime between these two. For the two-phase flow regimes, the commonly used two-phase multiplier concept is adopted. As they are somewhat standard approaches, details are not presented in the paper. More details are available in the RELAP5-3D code manual [9].

The model for interfacial friction has been simplified in this paper in order to improve the robustness of the computer code. In the previous paper [5], the interfacial friction model follows that of the RELAP5-3D code, e.g., drift flux model is used for vertical bubbly and slug flow regimes, and the drag coefficient model is used in all other flow regimes. In this paper, the model has been simplified to use the drift flux model in all vertical flow regimes, as the EPRI drift flux model provides a full coverage on the entire void fraction region. In addition, no significant changes in void fraction profiles were found in numerical results compared to the previous paper (discussed later). For all the flow regimes, the interfacial friction term is calculated using the drift flux model,

$$F_{int} = C_{int} u_R |u_R| \tag{9}$$

where the interfacial drag coefficient, C_{int}, and relative velocity, u_R, are defined as,

$$C_{int} = \frac{\alpha_g \alpha_l^3 (\rho_l - \rho_g) g}{|V_{gj}| V_{gj}} \tag{10}$$

and

$$u_R = C_1 u_g - C_0 u_l \tag{11}$$

$$C_1 = \frac{1 - C_0 \alpha_g}{\alpha_l} \tag{12}$$

in which, V_{gj} is the weighted mean drift velocity, and C_0 is the distribution parameter. Both parameters are modeled using the EPRI drift flux model proposed by Chexal and Lellouche [10].

Compared to previous studies, the major contribution in this paper is the implementation of the wall heat transfer model. In this paper, both the single-phase and two-phase flow wall heat transfer before critical heat flux (CHF) models are considered and implemented. Figure 2 shows a flowchart of the wall heat transfer model implemented. Because pre-CHF conditions are considered only, the branch to the nucleate boiling has been simplified compared to the RELAP5-3D wall heat transfer flowchart. For single-phase heat transfer, the Dittus-Boelter correlation for turbulence flow is used. For nucleate boiling, the correlation proposed by Chen is used,

$$q''_w = h_{mac}(T_w - T_{sat})F + h_{mic}(T_w - T_{sat})S \tag{13}$$

The macroscopic convection heat transfer coefficient, h_{mac}, is calculated from the Dittus-Boelter correlation; and the microscopic boiling heat transfer coefficient, h_{mic}, is calculated from the Forster-Zuber correlation,

$$h_{mic} = 0.00122\left(\frac{k_l^{0.79}c_{p,l}^{0.45}\rho_l^{0.49}}{\sigma^{0.5}\mu_l^{0.29}h_{lg}^{0.24}\rho_g^{0.24}}\right)\Delta T_w^{0.24}\Delta p^{0.75} \tag{14}$$

where, ΔT_w is wall superheat, and Δp is the difference between saturation pressure corresponding to wall temperature and bulk pressure. For the Reynolds number factor (F) and suppression factor (S) in equation (13), their detailed definition is omitted here, which can be found in the RELAP5-3D code manual [9]. Note that equation (13) has been proposed for saturated boiling flow conditions. If subcooled nucleate boiling is modeled, equation (13) is used with two modifications: changing T_{sat} into T_l in the macroscopic convection term, and a correction factor is used for F [9].

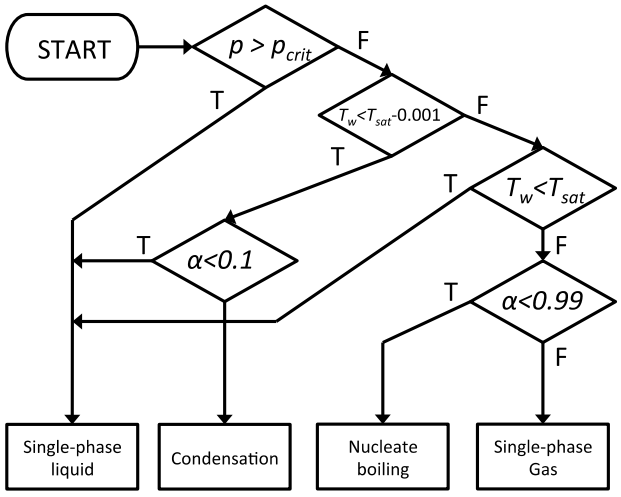

Figure 2, Flowchart for determining wall heat transfer modes for pre-CHF conditions.

3. NUMERICAL SCHEMES

3.1 Spatial Discretization Scheme

For the flow equations, staggered grid mesh arrangement has been used. As depicted in **Figure 1** (b), scalar variables (pressure, void fraction, and phasic temperatures) are arranged in cell centers, while vector variables (phasic velocities) are arranged on cell edges. For advection terms in flow equations, both the first-order and second-order upwind donor cell methods are implemented. The second-order

upwind spatial scheme is conceptually similar to the first-order one. It is obtained by introducing linear reconstructions of variable solutions into the original first-order upwind method. For the staggered grid arrangement, the advection terms in the gas phase mass equations are semi-discretized as,

$$\left.\frac{\partial(\alpha_g\rho_g u_g)}{\partial x}\right|_i = \frac{1}{\Delta x}\left[(\alpha_g\rho_g u_g)^*_{i+1/2} - (\alpha_g\rho_g u_g)^*_{i-1/2}\right] \tag{15}$$

If the traditional first-order upwind donor cell method is used, the mass flux on cell edge i+1/2 is numerically evaluated as,

$$(\alpha_g\rho_g u_g)^*_{i+1/2} = u_{g,i+1/2}\begin{cases}\alpha_{g,i}\rho_{g,i} & if \;\; u_{g,i+1/2} > 0\\ \alpha_{g,i+1}\rho_{g,i+1} & otherwise\end{cases} \tag{16}$$

Instead of the piecewise constant assumption in the first-order scheme, the second-order scheme requires an additional step to reconstruct piecewise linear distributions of variables in each finite volume cell. The mass flux on cell edge i+1/2 is then evaluated based on local edge velocity and the value of scalar variables on the cell edge (**Figure 3**),

$$(\alpha_g\rho_g u_g)^*_{i+1/2} = u_{g,i+1/2}\begin{cases}\alpha^-_{g,i+1/2}\rho^-_{g,i+1/2} & if \;\; u_{g,i+1/2} > 0\\ \alpha^+_{g,i+1/2}\rho^+_{g,i+1/2} & otherwise\end{cases} \tag{17}$$

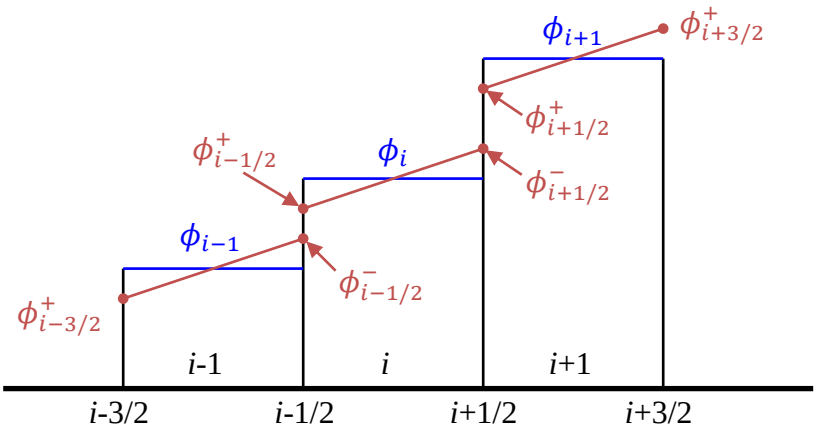

Figure 3, Schematic illustration of the linear reconstruction of variables using the slope limiter method. ϕ is the piecewise constant variables before linear reconstruction. $\phi^{+/-}$ is the reconstructed variables on cell edges after the linear reconstruction.

The same approach is used for the advection and the $\partial(\alpha u)/\partial x$ terms in the energy equation. The discretization of the advection term in the momentum equations is done slightly differently as it is formulated in primitive form. For the first-order upwind scheme, it is discretized as,

$$u_g\left.\frac{\partial u_g}{\partial x}\right|_{i+1/2} = \frac{1}{\Delta x}u_{g,i+1/2}\begin{cases}u_{g,i+1/2} - u_{g,i-1/2} & if \;\; u_{g,i+1/2} > 0\\ u_{g,i+3/2} - u_{g,i+1/2} & otherwise\end{cases} \tag{18}$$

While for the second-order version, the discretization is obtained by replacing the donor values with linearly reconstructed cell edge values,

$$u_g\left.\frac{\partial u_g}{\partial x}\right|_{i+1/2} = \frac{1}{\Delta x}u_{g,i+1/2}\begin{cases}u^-_{i+1} - u^-_i & if \;\; u_{g,i+1/2} > 0\\ u^+_{i+1} - u^+_i & otherwise\end{cases} \tag{19}$$

The linear reconstructions of variables are done using the slope limiter concept. For example, the reconstruction of scalar variable in the i^{th} volume can be done as,

$$\phi_{i+1/2}^{-} = \phi_i + \frac{\Delta x}{2}\phi_{x,i} \tag{20}$$

in which, $\phi_{x,i}$ is the reconstructed slope, which can be obtained by any standard slope limiter schemes, such as the Van Albada slope limiter used in this paper [11].

3.2 Discretized Forms

The discretized forms of the two-phase flow equation system, using BDF1 time integration scheme, are summarized as follows:

$$\frac{\alpha_{l,i}^{n+1}\rho_{l,i}^{n+1} - \alpha_{l,i}^{n}\rho_{l,i}^{n}}{\Delta t} + \frac{1}{\Delta x}\left[(\alpha_l\rho_l u_l)_{i+1/2}^{n+1,*} - (\alpha_l\rho_l u_l)_{i-1/2}^{n+1,*}\right] + \Gamma_{g,i}^{n+1} = 0 \tag{21}$$

$$\frac{\alpha_{g,i}^{n+1}\rho_{g,i}^{n+1} - \alpha_{g,i}^{n}\rho_{g,i}^{n}}{\Delta t} + \frac{1}{\Delta x}\left[(\alpha_g\rho_g u_g)_{i+1/2}^{n+1,*} - (\alpha_g\rho_g u_g)_{i-1/2}^{n+1,*}\right] - \Gamma_{g,i}^{n+1} = 0 \tag{22}$$

$$\begin{aligned}\bar{\alpha}_{l,i+1/2}^{n+1}\bar{\rho}_{l,i+1/2}^{n+1}\frac{u_{l,i+1/2}^{n+1} - u_{l,i+1/2}^{n}}{\Delta t} + \bar{\alpha}_{l,i+1/2}^{n+1}\bar{\rho}_{l,i+1/2}^{n+1}u_{l,i+1/2}^{n+1}\frac{\left[(u_l)_{i+1}^{n+1,*} - (u_l)_{i}^{n+1,*}\right]}{\Delta x} \\ + \bar{\alpha}_{l,i+1/2}^{n+1}\frac{p_{i+1}^{n+1} - p_i^{n+1}}{\Delta x} - \frac{1}{2}\left(\alpha_{l,i}^{n+1}\rho_{l,i}^{n+1}g_{x,i}^{n+1} + \alpha_{l,i+1}^{n+1}\rho_{l,i+1}^{n+1}g_{x,i+1}^{n+1}\right) - F_{int,i+\frac{1}{2}}^{n+1} \\ + \frac{1}{2}\left(F_{wall,l,i}^{n+1} + F_{wall,l,i+1}^{n+1}\right) + \Gamma_{g,i+1/2}^{n+1,*}\left(u_{int,i+1/2}^{n+1} - u_{l,i+1/2}^{n+1}\right) = 0\end{aligned} \tag{23}$$

$$\begin{aligned}\bar{\alpha}_{g,i+1/2}^{n+1}\bar{\rho}_{g,i+1/2}^{n+1}\frac{u_{g,i+1/2}^{n+1} - u_{g,i+1/2}^{n}}{\Delta t} + \bar{\alpha}_{g,i+1/2}^{n+1}\bar{\rho}_{g,i+1/2}^{n+1}u_{g,i+1/2}^{n+1}\frac{\left[(u_g)_{i+1}^{n+1,*} - (u_g)_{i}^{n+1,*}\right]}{\Delta x} \\ + \bar{\alpha}_{g,i+1/2}^{n+1}\frac{p_{i+1}^{n+1} - p_i^{n+1}}{\Delta x} - \frac{1}{2}\left(\alpha_{g,i}^{n+1}\rho_{g,i}^{n+1}g_{x,i}^{n+1} + \alpha_{g,i+1}^{n+1}\rho_{g,i+1}^{n+1}g_{x,i+1}^{n+1}\right) \\ + F_{int,i+\frac{1}{2}}^{n+1} + \frac{1}{2}\left(F_{wall,g,i}^{n+1} + F_{wall,g,i+1}^{n+1}\right) - \Gamma_{g,i+1/2}^{n+1,*}\left(u_{int,i+1/2}^{n+1} - u_{g,i+1/2}^{n+1}\right) = 0\end{aligned} \tag{24}$$

$$\begin{aligned}\frac{\alpha_{l,i}^{n+1}\rho_{l,i}^{n+1}e_{l,i}^{n+1} - \alpha_{l,i}^{n}\rho_{l,i}^{n}e_{l,i}^{n}}{\Delta t} + \frac{1}{\Delta x}\left[(\alpha_l\rho_l u_l e_l)_{i+1/2}^{n+1,*} - (\alpha_l\rho_l u_l e_l)_{i-1/2}^{n+1,*}\right] + p_i^{n+1/2}\frac{\alpha_{l,i}^{n+1} - \alpha_{l,i}^{n}}{\Delta t} \\ + p_i^{n+1}\frac{1}{\Delta x}\left[(\alpha_l u_l)_{i+1/2}^{n+1,*} - (\alpha_l u_l)_{i-1/2}^{n+1,*}\right] - Q_{wl,i}^{n+1} - Q_{il,i}^{n+1} + \Gamma_{ig,i}^{n+1}h_{l,i}^{n+1,*} \\ + \Gamma_{w,i}^{n+1}h_{l,i}^{n+1,\prime} = 0\end{aligned} \tag{25}$$

$$\begin{aligned}\frac{\alpha_{g,i}^{n+1}\rho_{g,i}^{n+1}e_{g,i}^{n+1} - \alpha_{g,i}^{n}\rho_{g,i}^{n}e_{g,i}^{n}}{\Delta t} + \frac{1}{\Delta x}\left[(\alpha_g\rho_g u_g e_g)_{i+1/2}^{n+1,*} - (\alpha_g\rho_g u_g e_g)_{i-1/2}^{n+1,*}\right] \\ + p_i^{n+1/2}\frac{\alpha_{g,i}^{n+1} - \alpha_{g,i}^{n}}{\Delta t} + p_i^{n+1}\frac{1}{\Delta x}\left[(\alpha_g u_g)_{i+1/2}^{n+1,*} - (\alpha_g u_g)_{i-1/2}^{n+1,*}\right] - Q_{wg,i}^{n+1} \\ - Q_{ig,i}^{n+1} - \Gamma_{ig,i}^{n+1}h_{g,i}^{n+1,*} - \Gamma_{w,i}^{n+1}h_{g,i}^{n+1,\prime} = 0\end{aligned} \tag{26}$$

where, $\rho_{l,i} = \rho_l(p_i, T_{l,i})$, $e_{l,i} = e_l(p_i, T_{l,i})$. $\bar{\alpha}_{l/g,i+1/2}^{n+1}$ and $\bar{\rho}_{l/g,i+1/2}^{n+1}$ are edge averaged values from its two neighboring cells. Replacing BDF1 scheme with BDF2 scheme would be straightforward. Compared to the previous study [5], one major difference presented in this paper is the treatment on the interfacial drag term. At first, drift flux model has been used for all vertical flow regimes as explained in section 2.2.

For the numerical discretization, the values of C_0, C_1, V_{gj}, and C_{int}, are all evaluated using local edge values. This approach is taken to simplify the code implementation, as well as to improve the solver robustness.

The discretization of the two-dimensional heat conduction equation uses the standard second-order finite differencing method. By assuming constant properties and dropping the subscript 's' (for solid) and 'n+1' for most terms, the discretized equation reads,

$$\left(\rho c_p\right)_{i,j} \frac{T_{i,j}^{n+1} - T_{i,j}^{n}}{\Delta t} - k_{i,j}\left[\frac{T_{i-1,j} - 2T_{i,j} + T_{i+1,j}}{(\Delta x)^2} + \frac{T_{i,j-1} - 2T_{i,j} + T_{i,j+1}}{(\Delta y)^2}\right] - q'''_{i,j} = 0 \qquad (27)$$

The coupling between the solid heat conduction equation and the two-phase flow energy equation is via the boundary condition of the heat conduction equation and the wall heat terms in the energy equation. For example, in saturated flow boiling, all wall heat is assumed to deposit into the liquid phase, i.e., the Q_{wl} term in the liquid-phase energy equation. The following steps ensure the correct coupling and energy conservation of the conjugate heat transfer. At first, wall heat flux is evaluated from equation (13). The wall heat transfer term at the i^{th} cell, $Q_{wl,i}$, is then calculated as $Q_{wl,i} = q''_{w,i} a_{w,i}$, in which a_w is the heating surface area per unit volume. At last, $q''_{w,i}$ is applied to the solid heat conduction equation as the boundary condition, such that,

$$-k_{i,j} \frac{T_{i,N} - T_{i,N-1}}{\Delta y} = q''_{w,i} \qquad (28)$$

Here we let $q''_{w,i}$ be positive when heat is transferred from the solid heat structure to the fluid. The discretized equations summarized in this section represent the nonlinear equations systems that are solved with the Newton-Krylov method. A detailed description of the JFNK method has been provided in [5], and therefore is omitted in this paper.

4. NUMERICAL RESULTS AND DISCUSSIONS

Similar to previous studies, numerical results were validated with existing experimental data, i.e., the Bartolomei data in vertical pipes [12] and FRIGG data in vertical bundles [13, 14]. Since there are no wall temperature and phasic velocities measurements available in these data, the RELAP5-3D system analysis code [9], was also used to benchmark the numerical results obtained in this work.

4.1. Validation

In our previous studies, both the Bartolomei flow boiling data in vertical pipes and FRIGG FT-36b flow boiling data in vertical bundles have been used for validation purpose [5]. As described in sections 2.2 and 3.2, both the closure correlation for interfacial drag and numerical discretization have been modified in this paper. It is therefore necessary to estimate how they affect numerical results, and to ensure that these numerical results are still with good accuracy comparing to experimental data. Both sets of experiments provide void fraction data at the steady state only, which will be used as the single quantity for the validation purpose.

The Bartolomei experiments were conducted using tubes with 12 mm inner diameter, 2 mm tube wall thickness, and 1.5 m heated length oriented vertically. These experiments covered a wide range of thermal-hydraulics conditions: 1) pressure from 3 to 15 MPa, 2) mass flux from 405 to 2123 kg/(m^2s), 3) wall heat flux from 0.42 to 2.21 MW/m^2, 4) inlet subcooling level from 11 to 140 K, and 5) maximum outlet void fraction up to 0.6. According to the discussion in the original paper, the maximum absolute errors of the void fraction measurements do not exceed ±0.04. The FRIGG tests consist of a series of tests with different loop configurations and thermal-hydraulics conditions. In this work, ten data sets from the FRIGG FT-36b series are used for code validation. For the FT-36b test, the test loop consisted of 36 rods with 4.365 m uniformly heated length and 13.8 mm outer diameter. An additional unheated rod with 20

mm outer diameter was present in the center of the rod bundle. All rods are housed in a cylinder shroud, with 159.5 mm inner diameter. It was documented in the original report that the absolute measurement error of void fraction is 0.003, by comparing void fraction measurements with known void fraction in a mock-up facility.

The 25 sets of Bartolomei data and 10 sets of FRIGG FT-36b data used in this work are the same data sets used in the previous work [5]. In this work, numerical results were obtained for all cases at the steady-state condition, using 20 finite volume cells, time step size $\Delta t = 0.2\ s$, and number of time steps $N_t = 200$. Numerical results on void fraction for several selected cases are presented in **Figure 4** and **Figure 5**, with comparisons to numerical results obtained in the previous work and experimental data. At first, since the closure correlation changes only apply to the interfacial drag of the annular mist flow regime that normally happens at large void fraction region, it is expected that void fraction prediction will be affected only in such large void fraction region. This is evident as shown in **Figure 5** that visible changes in void fraction prediction are present, while as shown in **Figure 4** the changes are small. In the large void fraction region, numerical results obtained in this work seem to give better agreement with experimental data. Moreover, **Figure 4** also indicates that the changes made in numerical discretization of interfacial drag term only have insignificant impact on numerical results. Overall, the numerical results obtained in this work are almost identical to those obtained in our previous work that have been well validated, with the exception that in larger void fraction region the improved accuracy is found.

4.2. Benchmark with RELAP5-3D Results

Both the Bartolomei and FRIGG data did not provide measurements on quantities such as wall temperature and fluid velocities. In order to validate the wall heat transfer correlations implemented, we have to rely on existing system analysis codes, such as the RELAP5 code, as benchmark references. The RELAP5 code was developed as a best-estimate reactor safety analysis code, which has been extensively validated and accepted as a *de facto* standard for reactor safety analysis. For several selected cases, numerical results obtained in this work are compared with RELAP5-3D results in figures 6 to 11. It is noted that semi-implicit method and first-order upwind spatial discretization scheme are both used in the RELAP5-3D code. For fair comparisons, the first-order BDF1 method and the same first-order upwind spatial discretization scheme were used to generate numerical results for comparisons. In general, it shows fairly good agreement between numerical results obtained in this work and those from RELAP5-3D code. For most cases, the difference in void fraction prediction is small, with exception in case 413-117. For all the cases, the predicted liquid phase temperatures agree almost perfectly with the RELAP5-3D results. The difference in wall temperature prediction is also small. Predicted phasic velocities are also similar between these two sets of numerical results. However, it has to be pointed out that we choose to present the velocity of the absent vapor phase differently than that of RELAP5-3D, where the absent vapor phase velocity is set to be the same as the liquid phase velocity in the single-phase liquid region. For this reason, the RELAP5-3D vapor-phase velocity jumps from the single-phase liquid regime to the two-phase flow regime, while a continuous vapor-phase velocity is shown in our results.

Overall, the comparison of numerical results of this work and those from RELAP5-3D shows good agreement between them. There are some slight difference between them, which are likely from the different closure correlations and numerical discretization used in this work.

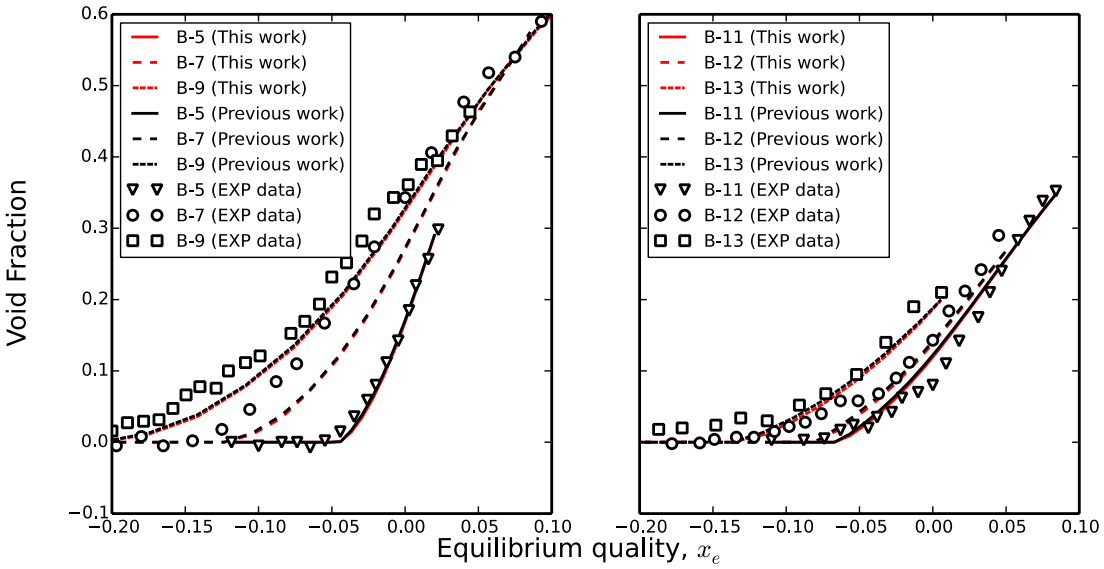

Figure 4, Comparison between numerical results of this work, of previous work, and experimental data for selected Bartolomei tests.

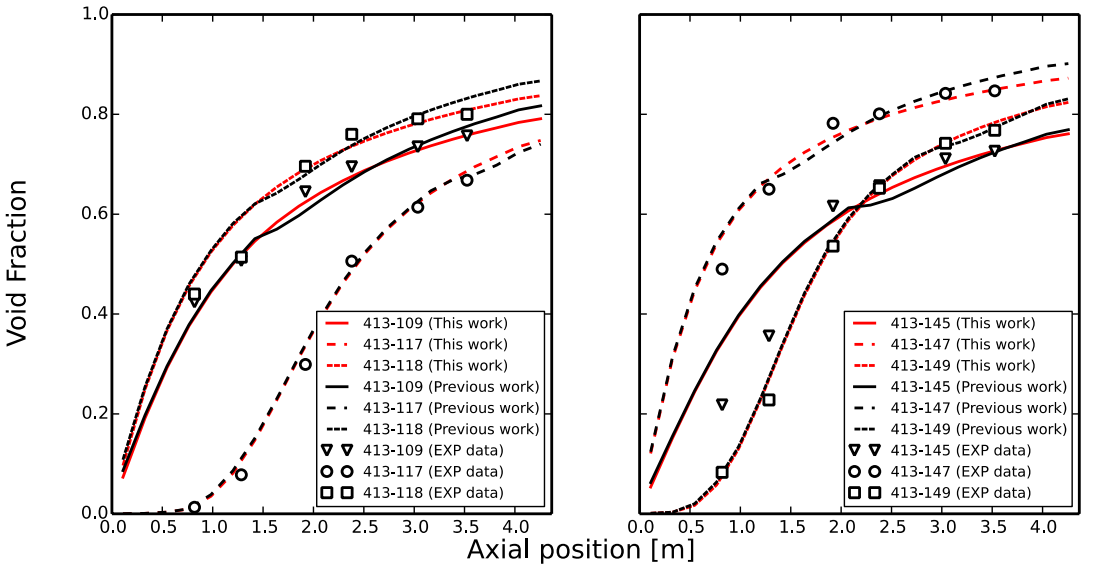

Figure 5, Comparison between numerical results of this work, of previous work, and experimental data for selected FRIGG FT-36b test.

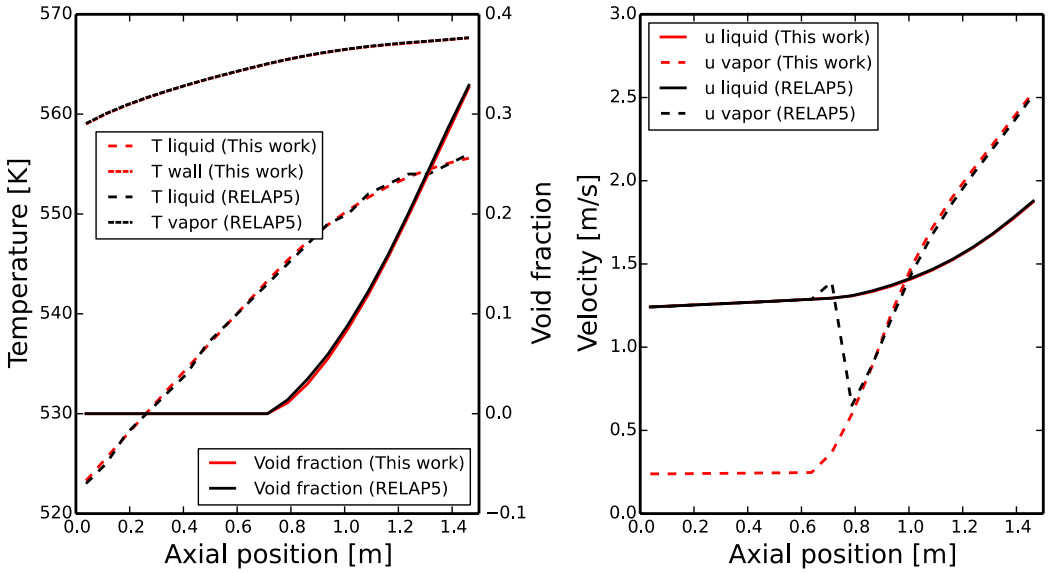

Figure 6, Comparison between numerical results of this work and results from RELAP5-3D code, for the Bartolomei case-5.

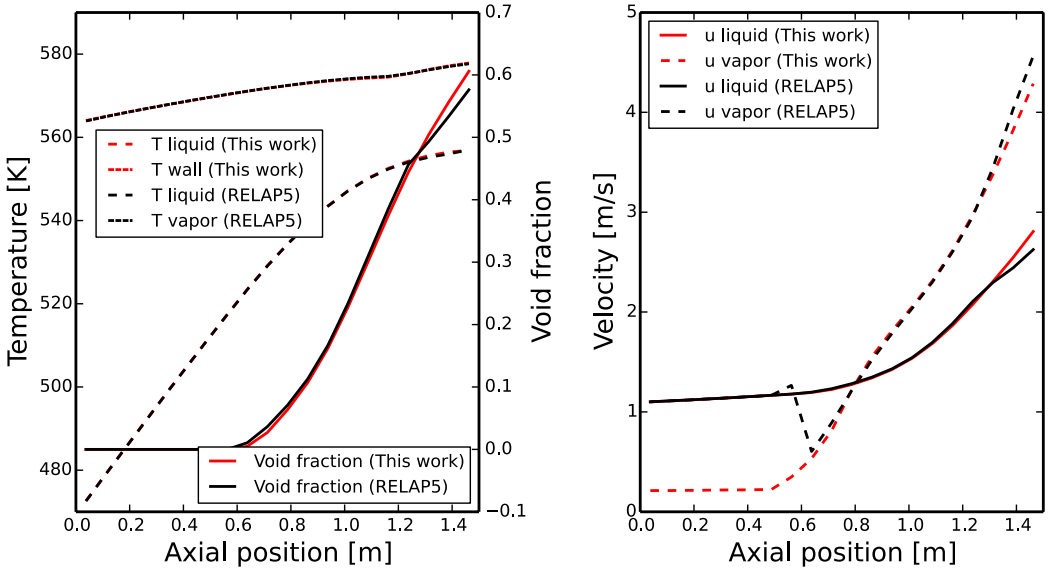

Figure 7, Comparison between numerical results of this work and results from RELAP5-3D code, for the Bartolomei case-7.

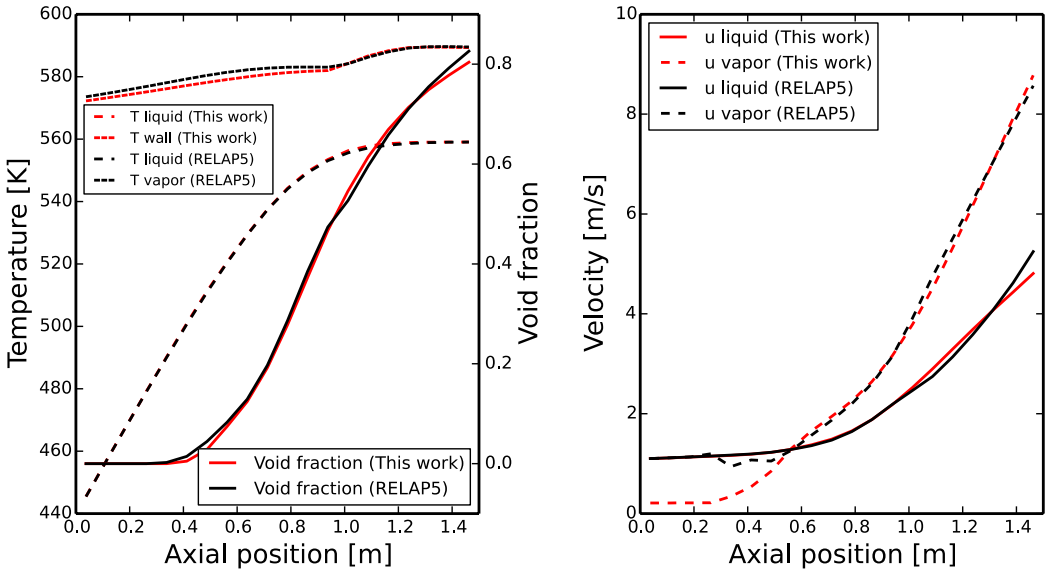

Figure 8, Comparison between numerical results of this work and results from RELAP5-3D code, for the Bartolomei case-9.

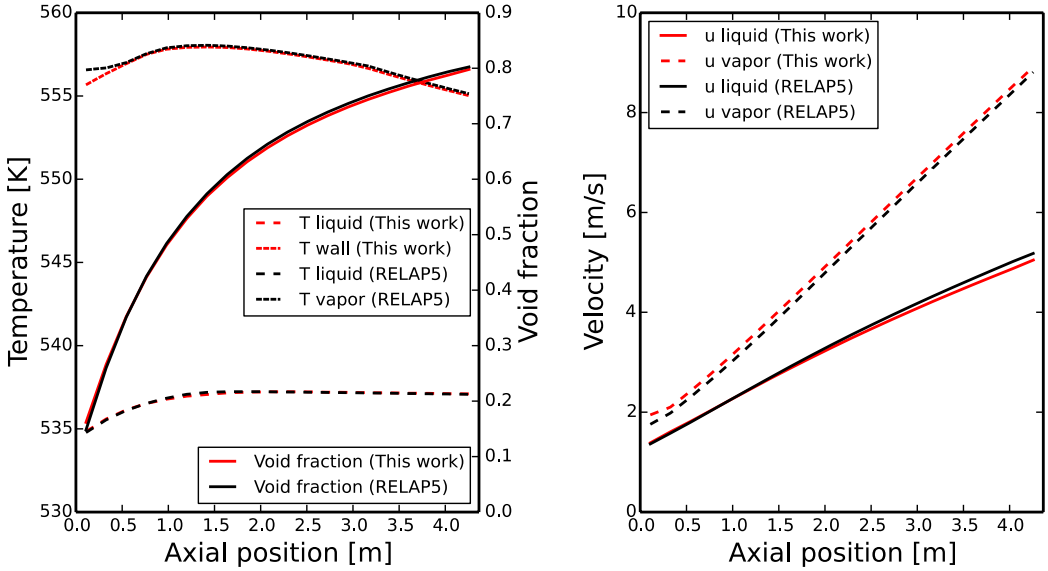

Figure 9, Comparison between numerical results of this work and results from RELAP5-3D code, for the FRIGG FT-36b test 413-109.

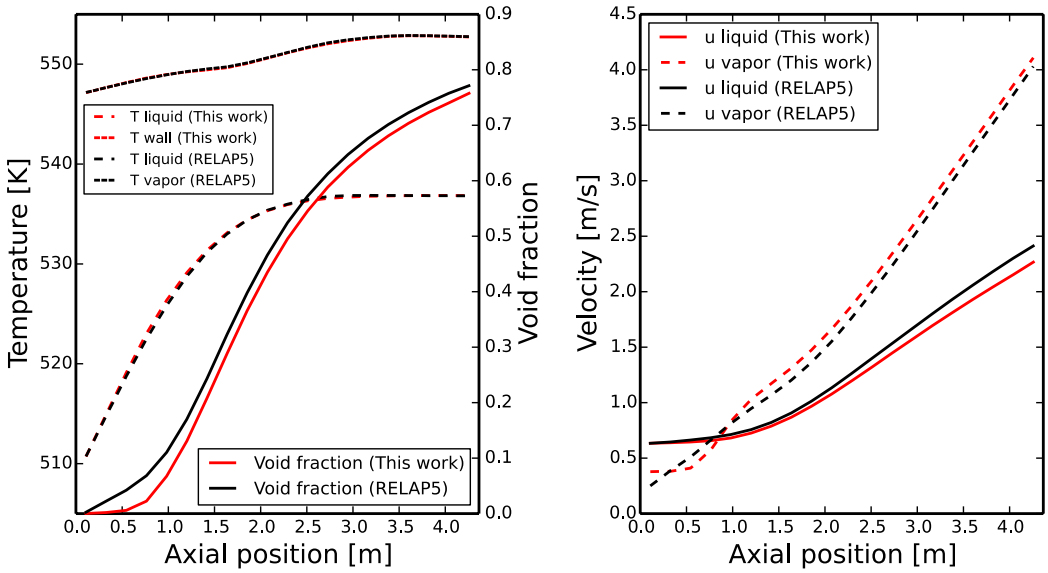

Figure 10, Comparison between numerical results of this work and results from RELAP5-3D code, for the FRIGG FT-36b test 413-117.

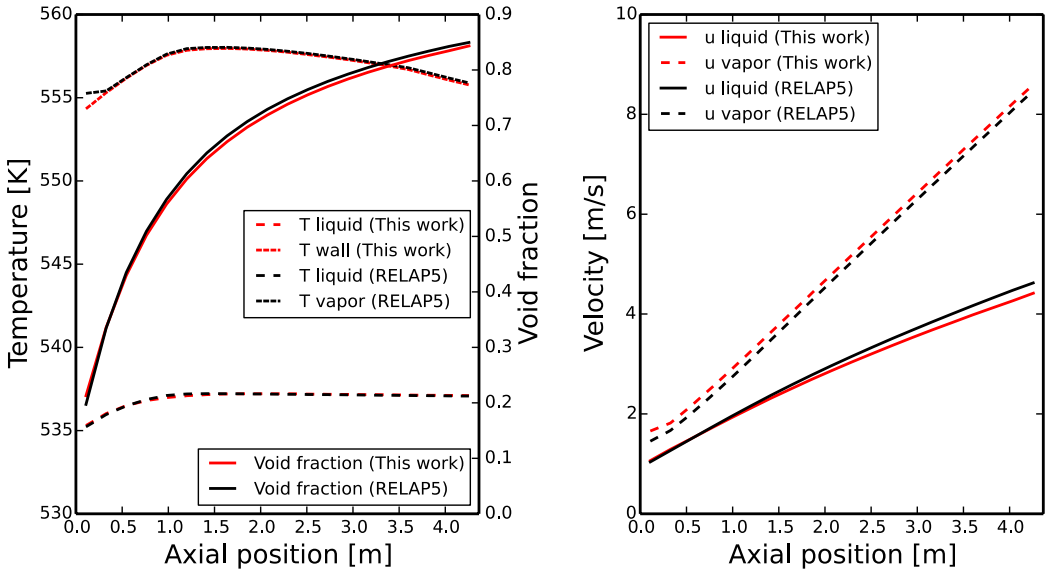

Figure 11, Comparison between numerical results of this work and results from RELAP5-3D code, for the FRIGG FT-36b test 413-118.

5. CONCLUSIONS

In this paper, an extended study has been performed to include the two-dimensional heat conduction model that is coupled to the two-phase flow model through wall heat transfer. The coupled conjugate heat transfer problem is solved in a fully implicit and fully coupled manner, using the Jacobian-free Newton Krylov (JFNK) method as the nonlinear solver. Because of the discontinuous nature of closure correlations used, for example discrete flow regimes and discrete modes in wall heat transfer models, several treatments were introduced to improve the robustness of the JFNK method. Compared to the

previous work, a transition region is re-introduced between the slug and annular mist flow regimes, which is however limited to be 0.01 in void fraction and applied to interfacial heat transfer only. The width of this transition region in void fraction has also been greatly reduced compared to 0.05 used in RELAP5-3D. The closure correlations for interfacial drag have also been slightly simplified, as only the drift flux model is used.

Both validation with experimental data and benchmark with the RELAP5-3D code were performed. Compared to our previous studies, the modifications mentioned above did not introduce any significant changes in numerical results, because these modifications are somewhat minor. Code-to-code benchmark with the RELAP5-3D code further verifies the correct implementation of conjugate heat transfer between solid heat structure and fluid flow.

ACKNOWLEDGMENTS

This work is supported by the U.S. Department of Energy, under Department of Energy Idaho Operations Office Contract DE-AC07-05ID14517. Accordingly, the U.S. Government retains a nonexclusive, royalty-free license to publish or reproduce the published form of this contribution, or allow others to do so, for U.S. Government purposes.

REFERENCES

1. U.S. Nuclear Regulatory Commission, "RELAP5/MOD3.3 Code Manual Volume I," NUREG/CR-5535 ed., December, (2001).
2. V.A. Mousseau, "Accurate Solution of the Nonlinear Partial Differential Equations from Thermal Hydraulics," *Nuclear Technology*, **158**, pp. 26-35 (2005).
3. L. Zou, H. Zhao, H. Zhang, "Solving phase appearance/disappearance two- phase flow problems with high resolution staggered grid and fully implicit schemes by Jacobian-free Newton–Krylov method," *Computers and Fluids*, **129**, pp. 179-188 (2016).
4. L. Zou, H. Zhao, H. Zhang, "Implicitly solving phase appearance and disappearance problems using two-fluid six-equation model," *Progr. Nucl. Energy*, **88**, pp. 198–210 (2016).
5. L. Zou, H. Zhao, H. Zhang, "Application of Jacobian-Free Newton-Krylov Method in Implicitly Solving Two-Fluid Six-Equation Two-phase Flow Problems: Implementation, Validation and Benchmark," *Nuclear Engineering and Design*, **300**, pp. 268-281 (2016).
6. U.S. Nuclear Regulatory Commission, "TRAC-M/FORTRAN 90 (Version 3.0) Theory Manual", NUREG/CR-6724 ed., April, (2001b).
7. U.S. Nuclear Regulatory Commission, "TRACE V5.0 Theory Manual, Field Equations, Solution Methods, and Physical Models," (2010)
8. D. Bestion, "The physical closure laws in the CATHARE code," *Nucl. Eng. and Des.*, **124**, pp. 229-245 (1990).
9. Idaho National Laboratory, "RELAP5-3D Code Manual Volume I: Code Structure, System Models and Solution Methods," INEEL-EXT-98-00834, Revision 4.0, June (2012).
10. B. Chexal and G. Lellouche, "A Full-Range Drift-Flux Correlation for Vertical Flows (Revision 1)," EPRI NP-3989-SR, Electric Power Research Institute, September (1986).
11. E.F. Toro, *Riemann Solvers and Numerical Methods for Fluid Dynamics: A Practical Introduction*, Springer Science & Business Media, (2009).
12. G.G. Bartolomei, et al., "An Experimental Investigation of True Volumetric Vapor Content with Sub-cooled Boiling in Tubes," *Thermal Engineering* **29** (3), 132–135, (1982).
13. O. Nylund, et al., "Hydrodynamic and Heat Transfer Measurements on a Full-Scale Simulated 36-Rod Marviken Fuel Element with Non-uniform Radial Heat Flux Distribution," FRIGG Loop Project, FRIGG-3, (1969).
14. J.A. Skaug, R. Eklund, and O. Nylund, "FT-36b: Results of Void Measurements," FRIGG Loop Project, FRIGG-PM--15, (1968).